Article:
Bustos-Ramirez, G., Graves, J. P. orcid.org/0000-0002-7959-7959 and Brunetti, D. (2025) Extending the space of edge harmonic oscillations by magnetic symmetry breaking external coils in tokamaks. Plasma Physics and Controlled Fusion. 095005. ISSN: 1361-6587

https://doi.org/10.1088/1361-6587/adfe92

PAPER • **OPEN ACCESS**

Extending the space of edge harmonic oscillations by magnetic symmetry breaking external coils in tokamaks

To cite this article: G Bustos-Ramirez *et al* 2025 *Plasma Phys. Control. Fusion* **67** 095005

OPEN ACCESS
IOP Publishing
Plasma Physics and Controlled Fusion
Plasma Phys. Control. Fusion **67** (2025) 095005 (16pp)
https://doi.org/10.1088/1361-6587/adfe92

Extending the space of edge harmonic oscillations by magnetic symmetry breaking external coils in tokamaks

G Bustos-Ramirez[1,*], J P Graves[2,3] and D Brunetti[4]

[1] Department of Applied Physics and Applied Mathematics, Columbia University, New York, NY 10027, United States of America
[2] School of Physics, Engineering and Technology, York Plasma Institute, University of York, York, Heslington YO10 5DD, United Kingdom
[3] École Polytechnique Fédérale de Lausanne (EPFL), Swiss Plasma Center (SPC), CH-1015 Lausanne, Switzerland
[4] UKAEA (United Kingdom Atomic Energy Authority), Culham Campus, Abingdon, Oxfordshire OX14 3DB, United Kingdom

E-mail: gbustosr@pppl.gov

Received 28 April 2025, revised 17 August 2025
Accepted for publication 22 August 2025
Published 3 September 2025

Abstract

This work presents numerical and analytic approaches for calculating the amplitude of edge harmonic oscillations (EHOs) associated with Quiescent H-modes in the presence of symmetry breaking magnetic coils. The analytic approach uses a linear ideal MHD model for EHOs and external kink modes subject to a given boundary condition defined by an externally applied helical field. The imposed 3D field is found to extend the parameter space of unstable external kink modes and EHOs, also providing an amplitude for the MHD perturbation, including the edge corrugation. The saturated states obtained using the linear time-invariant MHD equations are compared with those obtained with the `VMEC` nonlinear free boundary code, where the error field correction coils (EFCCs) in JET-like geometry were added to obtain a self-consistent equilibrium solution including the plasma response. Quantitative and qualitative agreement is found between the saturated amplitude calculated analytically and with `VMEC` for the case of the external kink modes. Only qualitative agreement was found for the most complex case of the EHO amplitude, though saturated amplitudes in both approaches are of the same order of magnitude and follow a similar linear trend with applied current to the EFCCs. The results obtained in this paper may help the modelling of the plasma response for external saturated modes, as well as offer an attractive route for scenario development and control in tokamak devices.

Keywords: tokamak, magnetohydrodynamics, edge harmonic oscillations, resonant magnetic perturbations, external kink modes

* Author to whom any correspondence should be addressed.

1. Introduction

Given the increased risk that edge localised modes (ELMs) pose to the integrity of plasma facing components in tokamak devices, special attention has been directed to high performance operational regimes which are intrinsically ELM-free. One important of such operational modes is the quiescent H-mode (QH-mode) [1], a state that retains H-mode level of energy confinement while replacing ELMs by the more benign edge harmonic oscillations (EHOs). EHOs are 3D edge corrugations that keep the plasma on the boundary of the peeling-ballooning stability diagram by enhancing particle transport across the pedestal, where the edge transport barrier is located during H-mode operation. While QH-mode has been successfully achieved in many tokamaks today, it is desirable to access it robustly using a wide range of plasma actuators.

Non-axisymmetric magnetic perturbation (MP) coils are typically used in tokamak plasmas to avoid the triggering of dangerous instabilities such as ELMs [2] and resistive wall modes [3]. With the installation of resonant MP coil systems in numerous tokamaks today (including ITER), MP coils can be used for other purposes, particularly, to widen the parameter space of weakly 3D tokamak configurations with optimised confinement properties, such as QH-mode. A good understanding of the plasma response to the MPs is required to robustly access such states. Modelling and simulations of MPs using linear and nonlinear techniques has been extensively studied in the past decades [4–10], and a good comparison between the most used numerical modelling approaches is presented in [11, 12]. The plasma response on 3D saturated plasma states can be studied in a dynamic or in an equilibrium manner. In the dynamic technique, linear (or nonlinear) MHD equations are used to evolve the plasma from an equilibrium state where a small 3D MP is added to the system. In the equilibrium technique the MHD equations are solved self-consistently in the presence of a 3D MP. In this work we explore the linear and non-linear equilibrium approaches, the linear one using an analytic large aspect ratio model of a tokamak plasma, and the nonlinear one using the `VMEC` free-boundary code [13]. Both approaches presented here are based on solving the linear (or nonlinear) equilibrium ideal MHD equations in the presence of a non-axisymmetric magnetic component, so agreement in the limit of very small saturated amplitude is expected. Given the similarities of the linear eigenmode spectrum and the `VMEC` nonlinear radial saturated spectrum observed for some external instabilities (see [14–16]), it is perhaps not surprising that agreement can found even at moderate amplitude.

Three important physical effects are left out in the `VMEC` numerical model that could modify the plasma response to MPs: plasma resistivity, rotation and the presence of a resistive wall. In a typical discharge with resonant MPs, magnetic islands at the rational surfaces can interact with the resistive wall and slow down the plasma rotation, eventually leading to locked wall modes (if the island is large enough) and to the termination of the discharge. Previous studies comparing the equilibrium plasma response between linear MHD codes and the `VMEC` code concluded that the fundamental differences in the obtained results are mainly attributed to the insufficient resolution of the `VMEC` code to properly resolve the localised singular currents appearing at rational surfaces, which in turn would shield the plasma perturbation from going further into the plasma [8, 12, 17]. The work presented in this paper is focused on saturated external modes whose physical drive does not rely on an exact resonance within the plasma, thus avoiding the limitations in the `VMEC` code. The goal of this paper is twofold. Firstly, we aim to show that `VMEC` is a useful tool to study the plasma response to non-axisymmetric external perturbations if the physics studied is independent of the induced current at rational surfaces. This is done by comparing a very simple analytical external kink model with the 3D saturated states calculated in `VMEC`. Secondly, and once the first goal is demonstrated, a study the modification of the parameter space on saturated exfernal modes is presented, which have been theorised to be the EHOs observed during QH-mode operation in tokamak plasmas [15, 18]. This result could result in an important application since robust access to QH-mode in future machines could be aided by the application of MPs.

The paper is structured as follows. Section 2 presents the analytical and numerical models of the applied non-axisymmetric MPs. Section 3 applies both approaches to the case of saturated external kink modes, where a quantitative comparison is presented and shown to be in good agreement. Section 4 presents the application of MPs to the case of saturated exfernal modes, where a comparison between the two approaches is presented and the expansion of the parameter space for saturated exfernal modes is explored. Finally, section 5 presents a summary and conclusions of the work.

2. Models for the non-axisymmetric MPs

2.1. The antenna time-invariant linear model

The analytical model under consideration is a subset of the one reported by Lazzaro and Nave [4], where an external non-axisymmetric MP is introduced through a surface current located in the vacuum region, as shown in figure 1. The use of this simplified '*antenna*' model, rather than a magnetic field generated by realistic 3D coils, is justified by the assumption that only the MP component with the same helicity as the plasma mode significantly influences the plasma response. This assumption is supported by the results in [8] for external kink modes, and further validated in this study by the quantitative agreement on the saturated amplitude obtained the analytical model and with a nonlinear numerical simulation that employs full 3D coils.

The coordinate system (r,θ,ϕ) is used, where r labels flux surfaces, θ is the straight field line (SFL) poloidal angle and ϕ is the geometrical toroidal angle. The tokamak ordering is assumed:

$$\beta \sim \frac{2\mu_0 P}{B_0^2} \sim \epsilon^2, \quad \frac{B_p}{B_t} = \frac{\psi_p' |\nabla\phi \times \nabla r|}{|} |F\nabla\phi| \sim \epsilon, \quad q(r) \sim 1, \tag{1}$$

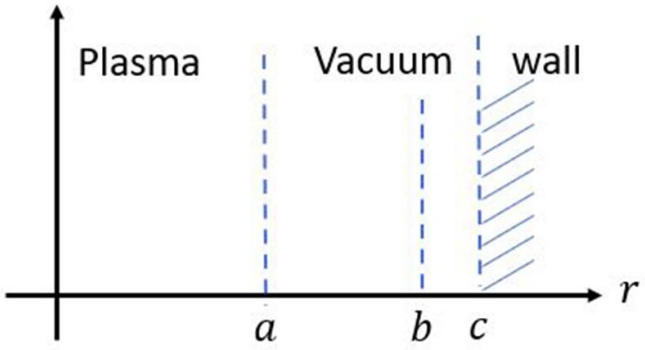

Figure 1. Diagram of the plasma system with an antenna at $r = b$.

where $\epsilon \equiv a/R_0 \ll 1$, with a and R_0 the minor and major radius respectively, ψ_p' is the radial derivative of the poloidal magnetic flux and $F = B_\phi$ is the covariant component of the magnetic field in the toroidal direction. The plasma region ($\in [0,a]$) is separated from an ideally conducting wall (located at $r = c$) by a vacuum region ($\in [a,c]$). At radius $r = b$ ($a < b < c$), an antenna with a current $I_A \propto \mathrm{e}^{\mathrm{i}(m\theta - n\phi)}$ provides a static helical perturbed magnetic field. The equation describing the perturbed vacuum magnetic flux for each independent poloidal mode is [4]

$$\nabla_\perp^2 \Psi_m(r,\theta,\phi) = \frac{\mu_0}{b} I_A \delta(r-b)\, \mathrm{e}^{\mathrm{i}(m\theta - n\phi)}. \tag{2}$$

The solutions in the regions $a < r < b$ and $b < r < c$ are given respectively by

$$\begin{aligned} \Psi_m^{(1)}(r) &= A_m (r/b)^m + B_m (r/b)^{-m} \\ \Psi_m^{(2)}(r) &= C_m (r/c)^m + D_m (r/c)^{-m}, \end{aligned} \tag{3}$$

where the constants are determined by the boundary conditions at the interfaces and current carrying layers, which read

$$\begin{aligned} \Psi^{(2)}(c) &= 0 \\ \Psi_m^{(1)}(a+\delta) &= \frac{B_0}{m}\frac{r}{R_0} k_\parallel(r)\, \xi_m(r)\Big|_{a-\delta} \\ \Psi_m^{(1)}(b-\delta) &= \Psi_m^{(2)}(b+\delta) \\ \left[\!\left[r\frac{\mathrm{d}}{\mathrm{d}r}\Psi_m \right]\!\right]_b &= \mu_0 I_A, \end{aligned} \tag{4}$$

where $k_\parallel = m/q - n$ is the dimensionless parallel wave number, B_0 is the plasma magnetic field evaluated at the magnetic axis, q is the safety factor and $\xi_m(r)$ is the radial saturated plasma displacement with the same helicity as the antenna. The first condition corresponds to the vanishing of the perturbed normal magnetic field at the ideal conducting wall. The second and third conditions are derived invoking the continuity of the normal magnetic field at the plasma-vacuum interface and at the antenna respectively. The fourth condition is found by integrating equation (2) across the antenna, which is the equivalent jump condition of the tangential perturbed field $\delta B_m^\theta = -\Psi_m'$. The constants A_m, B_m, C_m and D_m are respectively given by

$$\begin{aligned} A_m &= -\frac{(b/a)^m \left[H_m I_\xi + 2\epsilon (a/c)^{2m} k_{\parallel a}\right]}{2m\left[1-(a/c)^{2m}\right]} B_0 \xi_m(a) \\ B_m &= \frac{(b/a)^{-m} \left[H_m I_\xi + 2\epsilon k_{\parallel a}\right]}{2m\left[1-(a/c)^{2m}\right]} B_0 \xi_m(a) \\ C_m &= \frac{(b/c)^m \left[(a/b)^{2m}-1\right] I_\xi + 2\epsilon (a/c)^m k_{\parallel a}}{2\left[(a/c)^{2m}-1\right] m} B_0 \xi_m(a) \\ D_m &= -\frac{(b/c)^m \left[(a/b)^{2m}-1\right] I_\xi - 2\epsilon (a/c)^m k_{\parallel a}}{2\left[(a/c)^{2m}-1\right] m} B_0 \xi_m(a), \end{aligned} \tag{5}$$

where $\epsilon = a/R_0$, $I_\xi = \frac{I_A \mu_0}{B_0 \xi_m(a)}$ and $H_m = \left[1-(b/c)^{2m}\right](a/b)^m$. Note that the perturbed magnetic field is composed of two sources. The first one corresponds to the perturbed field generated by the saturated edge plasma corrugation ($\xi_m(a)$), and the second one corresponds to the non-axisymmetric field imposed externally. Therefore, the finite amplitude mode $\xi_m(a)$ which is in force balance with the applied non-axisymmetric field already contains the plasma response. In the limit of $\xi_m(a) \to 0$, the perturbed vacuum field corresponds to that of an helical winding current between two ideally conducting toroidal surfaces. Finally, we point out that the perturbed magnetic field from the antenna considers a single helical harmonic (m,n). In reality, non-axisymmetric coils used in fusion experiments contain a spectrum of harmonics, and coupling between them and the plasma perturbation is possible. Nevertheless, previous work shows that a single helical harmonic in SFL coordinates quite reasonably describes the plasma response [8]. This is also shown in the present paper for saturated external kink and exfernal modes. Note that the validity of the linear model is limited to cases where the axisymmetric plasma in the absence of MPs is stable due to the absence of inertial forces in the linear model that would drive the plasma out of force balance, as discussed in section 3.

2.2. The VMEC nonlinear model

The calculation of external saturated states in the VMEC free boundary equilibrium code [13] requires a description of the vacuum magnetic field. Such field is calculated through the Biot–Savart law from a series of one dimensional filaments carrying current using the MAKEGRID code from the STELLOPT package [19]. Since VMEC is a 3D code, the filaments are not restricted to axisymmetry and MPs can easily be included by just adding a set of non-axisymmetric coils. The plasma equilibrium in VMEC is calculated self-consistently with the MPs, and therefore the plasma response is already included in the solution. A JET-like set of coils is used as illustrated in figure 2, consisting of 32 toroidal coils, six poloidal coils and 4 error field correction coils (EFCCs), where the later ones

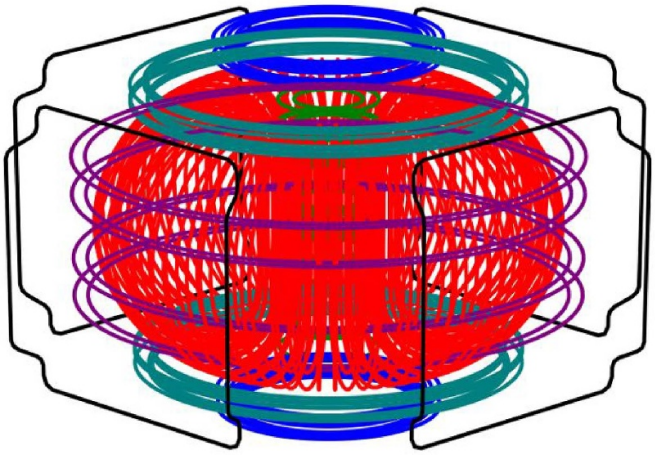

Figure 2. JET-like coil system, consisting on 32 toroidal coils (red), 6 poloidal coils (purple, green and blue) and 4 error field correction coils (black).

provide the non-axisymmetric perturbation. Toroidal and poloidal coils are made by four filaments carrying $1/4$ of the current, while the EFCCs are made by a single filament. In the JET tokamak, each EFCC contains 16 turns with a current capacity of 3 kA per turn [20], resulting in a total of 48 kA per coil. In order to compare the saturated states calculated in VMEC with those calculated analytically, it is necessary to characterise the vacuum MPs generated by the EFCCs.

While the VMEC code is able to calculate MHD equilibria without assuming any special symmetry, stellarator symmetry is chosen because the calculations are faster and have better convergence. In axisymmetric devices, stellarator symmetry is reduced to up-down symmetry, which is satisfied by the poloidal and toroidal coils in our set as shown in figure 2. The EFCC coils are modified to be an up-down symmetric approximation of the real set of JET coils in order to preserve stellarator symmetry. Figure 3(a) shows schematically the location of the EFCC coils in the tokamak system. Stellarator symmetry requires all scalar quantities, including current in the coils, to be mirrored about the $\phi = 0$ and $Z = 0$ planes. The current applied to coil number 1 (4) will be mirrored in coil number 2 (3), meaning that coils 1 and 2 (or 3 and 4) will flow in opposite directions, as shown in figure 3(b). With such coil configuration it is possible to apply a dominant $n_{\mathrm{EFCC}} = 1$ or $n_{\mathrm{EFCC}} = 2$ vacuum MP without breaking stellarator symmetry by changing the current pattern in coils 1 and 4, as shown in figure 3(b).

The perturbed toroidal spectrum of the magnetic field is dominated by a $n_{\mathrm{EFCC}} = 1$ or $n_{\mathrm{EFCC}} = 2$ mode due to the EFCCs, but a second source of non-axisymmetric field exist because of the finite number of toroidal coils, denominated as 'toroidal ripple'. In our JET-like coil set, the toroidal ripple has $n_{\mathrm{ripple}} = 32$ dominant toroidal mode number. Therefore, the most sensible choice for our study is to completely eliminate the toroidal ripple, which is done by choosing 32 (or 16) toroidal planes in the VMEC numerical grid so that each plane coincides with a toroidal coil, giving the effect of an axisymmetric vacuum field coming from the toroidal field coils (as shown in figure 4). A different choice of toroidal planes could result on incorrect numerical resolution of the magnetic field in VMEC due to aliasing. In the VMEC free-boundary code, the numerical grid considers a user-specified number of toroidal planes where the vacuum magnetic field is to be calculated. To correctly resolve such toroidal ripple the sampling points must satisfy the Nyquist criterion, so at least 64 toroidal planes are necessary along with the inclusion of 65 toroidal modes in the VMEC Fourier expansion. Note that 65 toroidal modes in a VMEC equilibrium calculation corresponds to the toroidal spectrum $-32 < n_{\mathrm{VMEC}} < 32$. The present study is not addressed to resolve the toroidal ripple nor the physics related with high-n modes. Moreover, simulations with a large number of toroidal modes generally do not converge well in VMEC and are extremely time consuming, so special care must be taken in deciding the appropriate number of toroidal planes used in the vacuum field calculation. For our JET-like set of coils, if the number of planes used is smaller than 64 (with the exception of 32,16,8,4,2), then the toroidal ripple will shift to an observable frequency due to aliasing. Figure 4 shows the toroidal spectrum of the radial perturbed magnetic field given by the toroidal field coils plus the EFCCs with 25, 32 and 80 planes in the VMEC numerical grid. It can be seen that using 25 coils shifts the toroidal ripple to $n_{\mathrm{ripple}} = 32 - 25 = 7$, and that this mode is of the same order than the $n_{\mathrm{EFCC}} = 1, 2$ produced by the EFCCs with 100 kA at the last closed flux surface (LCFS). Contrary to the perturbation produced by the EFCCs, the toroidal ripple decays quite fast when going towards the magnetic axis, where the ripple is negligible compared to the EFCCs perturbed field (as seen in figure 4). It is noted that these modes exist on the vacuum field, but whether they will be captured by the VMEC equilibrium calculation will depend on the number of toroidal modes included in the VMEC Fourier expansion. For example, in a VMEC simulation with 30 toroidal planes, a 'fictitious' $n_{\mathrm{ripple}} = 32 - 30 = 2$ vacuum perturbation will be included in the equilibrium calculation if $-2 < n_{\mathrm{VMEC}} < 2$ toroidal modes are allowed in the VMEC Fourier expansion. Here relies the importance to carefully choose the number of toroidal planes in the calculation of the vacuum field, specially when studying the effect of externally applied MPs.

The antenna model described in the analytical model only considers a single helical mode (m, n), while the EFCCs in our JET-like coil set have a wider toroidal and poloidal spectrum. To make a proper comparison with the analytical model, the poloidal *vacuum* spectrum in the VMEC simulations must be resolved in SFL coordinates. This is done by calculating the perturbed vacuum field from the EFCC coils alone using the MAKEGRID code. The cylindrical components of the obtained field $\left(\delta B^R, \delta B^Z, \delta B^\phi\right)$ are extracted at the location of the LCFS of a neighbouring axisymmetric VMEC equilibrium[5] $(R(S = 1, \theta_{\mathrm{SFL}}), Z(S = 1, \theta_{\mathrm{SFL}}))$, where θ_{SFL} is the SFL poloidal angle in VMEC and S is the radial coordinate,

[5] Given a 3D saturated equilibrium state, a *neighbouring axisymmetric equilibrium* is defined as the 2D equivalent equilibrium obtained by restricting $n = 0$ toroidal modes in the VMEC Fourier expansion. For more detailed information refer to [14].

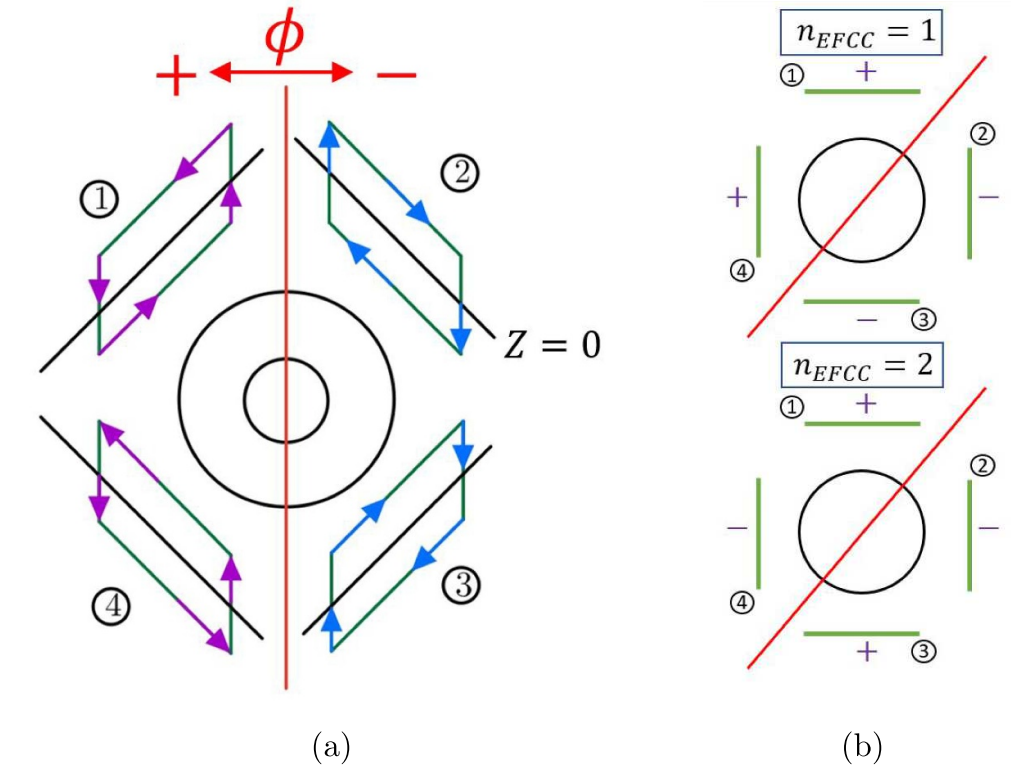

Figure 3. (a) Diagram of the EFCC of the JET-like set in `VMEC`. Stellarator symmetry means that the currents are mirrored with respect to the $\phi = 0$ plane (in red) and the $Z = 0$ plane (in black). Applied currents (in purple) in coils 1 and 4 are mirrored in coils 2 and 3 respectively (in blue). (b) Current patterns producing $n_{\mathrm{EFCC}} = 1$ (top) or $n_{\mathrm{EFCC}} = 2$ (bottom) dominant toroidal vacuum perturbations.

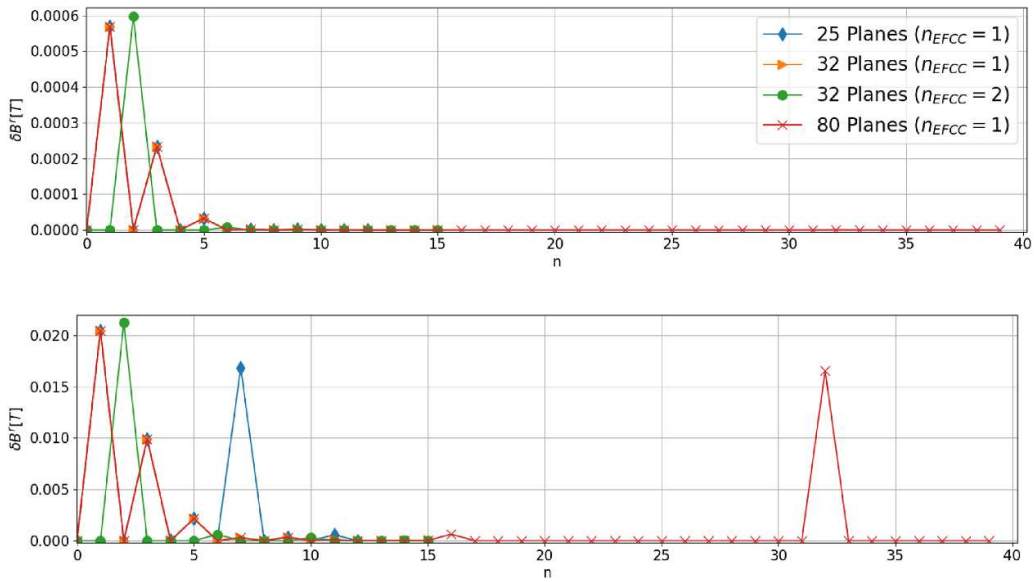

Figure 4. Toroidal Fourier decomposition of the vacuum magnetic field perturbation at the magnetic axis (up) and at the last closed flux surface (b) using different number of poloidal planes in the `VMEC` numerical grid. Note that the toroidal ripple shifts to an observable frequency if not enough planes are used. Also note that the toroidal ripple disappears if 32 planes are used. The current at the EFCCs was set to 100 kA for the calculation.

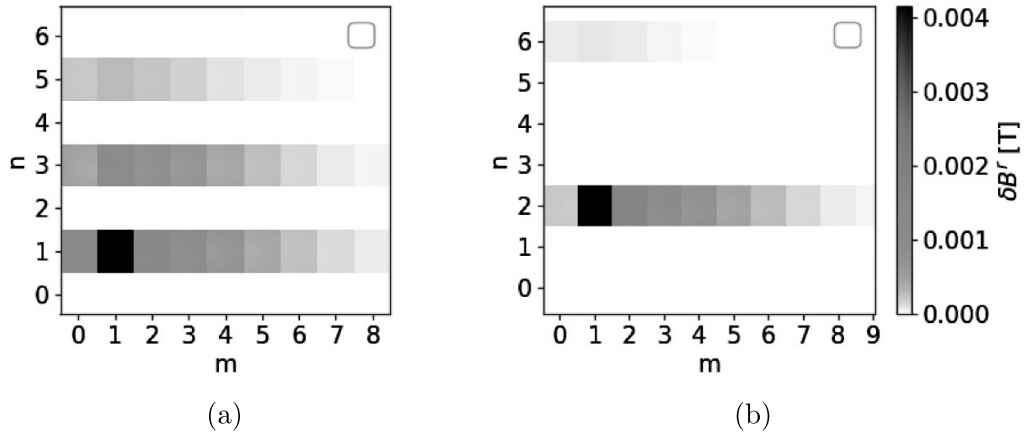

Figure 5. Poloidal and toroidal spectrum of the perturbed vacuum radial magnetic field $\delta B^r_{\mathrm{EFCC}}$ in SFL coordinates for (a) $n_{\mathrm{EFCC}} = 1$ and (b)$n_{\mathrm{EFCC}} = 2$ externally applied modes. Note that 32 toroidal planes in the VMEC numerical grid were used to eliminate the toroidal ripple.

which in VMEC can be chosen to be either the normalised toroidal or poloidal magnetic flux. The components of the perturbed vacuum magnetic field in flux coordinates are calculated through the transformation

$$\begin{pmatrix} \delta B^s \\ \delta B^\theta \\ \delta B^\phi \end{pmatrix} = \begin{pmatrix} \partial_s R & \partial_\theta R & 0 \\ \partial_s Z & \partial_\theta Z & 0 \\ 0 & 0 & R \end{pmatrix}^{-1} \begin{pmatrix} \delta B^R \\ \delta B^Z \\ \delta B^\phi \end{pmatrix}. \tag{6}$$

So that the vacuum EFCC field in the normal direction to the plasma

$$\delta B^r_{\mathrm{EFCC}} = \frac{R}{\mathcal{J}} \left[\frac{\partial Z}{\partial \theta} \delta B^R - \frac{\partial R}{\partial \theta} \delta B^Z \right] \frac{\mathrm{d}}{\mathrm{d}r} S. \tag{7}$$

Can be Fourier decomposed and compared to the analytical vacuum field from the antenna in the absence of a plasma

$$\delta B^r_{\mathrm{antenna}} = -\mathrm{i} \frac{H_m}{2a} \mu_0 I_A. \tag{8}$$

In equations (6) and (7), R and Z describe the flux surfaces in the neighbouring axisymmetric VMEC equilibrium, $\mathcal{J}$ is the corresponding Jacobian and $S = \psi/\psi_{\mathrm{edge}}$ is the radial VMEC flux function, which can be either the normalised toroidal or poloidal flux. Figure 5 shows the spectrum of $\delta B^r_{\mathrm{EFCC}}$ in SFL coordinates at the LCFS for a $n_{\mathrm{EFCC}} = 1$ and a $n_{\mathrm{EFCC}} = 2$ mode applied by the EFCCs. As can be seen, the amplitude of the mode decays with increasing poloidal mode number, although the $m = 1$ mode is dominant in both cases. Note that while $n_{\mathrm{EFCC}} = 2$ does have higher toroidal harmonics, they are only faintly visible on figure 5(b) due to the relative amplitude with the $n = 2$ component, which follows from the numerical solution of the Biot–Savart Law and the EFCC geometry. Even though the spectrum of the vacuum MP contains many harmonics, when comparing the VMEC results with analytic model it is assumed that only the vacuum component with the same helicity in SFL as the saturated edge mode has an effect in the final equilibrium state.

3. MP-induced saturated external kink modes

A non-resonant saturated external kink mode provides a valuable proof of concept for the comparison between the saturated states obtained with the VMEC code and our analytical predictions. Particularly, this is because this scenario avoids the formation of singular 'screening' currents and magnetic islands in response to MPs, allowing for a clean comparison between our two approaches. Moreover, it also connects directly to the broader physics discussed in this work, as the exfernal modes studied in section 4 are driven unstable by the coupling between an external kink drive and an infernal drive [16]. By first studying the plasma response of saturated external kink modes to MPs, we gain insight into the mechanisms that may underlie more complex coupled modes.

Finally, it represents the simplest experimentally relevant external mode, making it an ideal starting point for exploring the response of edge MHD instabilities to MPs. Saturated external kink modes in the presence of MPs have been investigated theoretically [21], and have been suggested to play a role in the suppression of edge localised modes (ELMs) in AUG and DIII-D discharges [9]. The present analysis offers a quantitative assessment of the external kink response using ideal MHD tools and linking it to the general framework developed in this manuscript.

3.1. Linear equilibrium equation for the analytic treatment of external kink modes with MP

Ideal MHD saturated states typically exist in a plasma as a consequence of the nonlinear evolution of a linearly unstable mode. Regardless of the dynamics leading to saturation, the final plasma state is a solution of the ideal MHD 3D equilibrium equation. For certain types of modes, the equilibrium solutions can be found using the *linearised* ideal MHD equilibrium equation. To lowest order, a time invariant perturbation

with mode number (m,n) satisfies Newcomb's equation [22]:

$$\frac{\mathrm{d}}{\mathrm{d}r}\left[r^3 k_\parallel^2 \frac{\mathrm{d}}{\mathrm{d}r}\xi_m\right] - r\left(m^2-1\right)k_\parallel^2 \xi_m = 0, \tag{9}$$

where $\xi_m(r)$ inside the plasma is fully determined by adequate boundary conditions, given by equations (3) and (4). Integrating equation (9) across the plasma-vacuum interface gives

$$\left[\!\left[k_\parallel^2 \frac{\mathrm{d}}{\mathrm{d}r}\xi_m\right]\!\right]_a = 0, \tag{10}$$

where $[]_a$ denotes jump conditions across $r=a$. We note that ξ_m' is discontinuous across the boundary since $\delta B_m^\theta = \psi_m' \sim \xi_m'$ corresponds to the jump of the tangential magnetic field. On the other hand, ξ_m is continuous across the boundary due to the continuity of the normal field ($\xi_m(a) \sim \delta B_m^r$), so we can divide the whole equation by the non-zero mode amplitude $\xi_m(a)$. On the vacuum side of $r=a$, we substitute $\xi_m = -\mathrm{i}\frac{R_0}{B_0 k_\parallel}\delta B_m^r\big|_{a+\delta}$, giving the equilibrium condition

$$k_\parallel^2(a)\left(\frac{r}{a}\left[\ln(\xi_m)\right]'\Big|_{a-\delta} - \left[ln\left(\frac{\delta B_m^r}{k_\parallel}\right)\right]'\Big|_{a+\delta}\right) = 0, \tag{11}$$

with two independent solutions

$$q(a) = m/n$$
$$\mathcal{B}_m = r\left[\ln\left(\frac{\delta B_m^r}{k_\parallel}\right)\right]'\Big|_{a+\delta}, \tag{12}$$

where $\mathcal{B}_m = r[\ln(\xi_m)]'|_{a-\delta}$ is typically calculated numerically from equation (9). The first solution is independent from the applied MP and corresponds to $k_\parallel(a)=0$, giving a resonance at the plasma edge. For such a solution, the plasma response to a helical displacement will drive a singular current at the boundary to screen the MP, which as discussed earlier, is not well represented in the VMEC code [17, 23]. Moreover, the assumed boundary conditions neglect surface currents, so the physics included in the present model is incomplete [6]. For these reasons, this work will not focus on the first equilibrium solution. The second equilibrium solution corresponds to the parenthesis term in equation (11) equal to zero, where we note that δB_m^r contains both the perturbed field due to the saturated edge plasma corrugation and from the antenna. Substituting the solution to the perturbed vacuum field (3) gives an equation for the function I_ξ

$$H_m I_\xi = -\frac{\epsilon\left[m\left(m-1+\mathcal{B}_m+(a/c)^{2m}(m+1-\mathcal{B}_m)\right)-(a/c)^{2m}(m-1-\mathcal{B}_m)nq_\mathrm{a}-(m+1+\mathcal{B}_m)nq_\mathrm{a}\right]}{mq_\mathrm{a}}, \tag{13}$$

where the right hand side only depends on equilibrium parameters without the application of the MPs and we recall that $I_\xi = \frac{I_A\mu_0}{B_0\xi_m(a)}$. Note that if $I_\xi = 0$, then the vacuum contribution equation for ideal external kink modes is exactly recovered [24, 25]. Equation (13) contains the solution to equations (2) and (9), and represents a plasma in equilibrium with a finite perturbation at the edge $\xi_m(a)$ when applying a current I_A to the antenna. One of the goals of this study is to verify this relation in the VMEC code, which will be achieved in section 3.2. Even though this work is dedicated to solve only for equilibrium states, it is useful to think of the problem in terms of the stability of the plasma in the absence of MPs. If the axisymmetric plasma is at marginal stability, then $I_A = 0$ is the only solution to equation (13) because the plasma is already in equilibrium to lowest order for an arbitrary perturbation amplitude. If the plasma is stable, then equation (13) will give the necessary current such that a saturated plasma perturbation with finite amplitude $\xi_m(a)$ remains in equilibrium with the perturbed field coming from the antenna. If the plasma is unstable, the linear analytical model predicts that the MPs would restore the plasma to force balance by creating a small amplitude external kink in equilibrium with the applied field perturbation. Note however that such scenario is not physical because the inertial forces that are in action when a finite growth rate is present are not captured by the linear equilibrium model [11].

Let us consider a Wesson-like current density profile $j_\phi(r) = j_0[1-(r/a)^2]^\nu$ [25], which gives $q(r) = \frac{q_\mathrm{a}(r/a)^2}{1-[1-(r/a)^2]^\nu}$ and $q_\mathrm{a}/q_0 = 1+\nu$. Consider also $a = 1.09$ m, $b = 3.8$ m, $c\to\infty$, $R_0 = 3.02$ m and $B_0 = 2.3$ T, which roughly correspond to the JET-like plasma discussed in the next section. For such profile, equation (9) has to be solved numerically in order to evaluate $\mathcal{B}_m$. By choosing $q_0 = 1.2$ an external kink with mode number $(m=3, n=1)$ is unstable in the region $2.95 < q_\mathrm{a} < 3$ in the absence of MPs. Figure 6 shows the evaluation of equation (13), where the necessary current to obtain a plasma equilibrium with saturated amplitude $\xi_m(a)$ is calculated as a function of the safety factor at the plasma boundary. It is found that a small amplitude saturated external kink mode can be induced with a modest current in the antenna over a region of the parameter space where an external kink is stable in the absence of MPs. Note that at marginal stability ($q_\mathrm{a} \sim 2.95$) all curves converge to zero current, which is the only equilibrium solution for an arbitrary amplitude mode, consistent with the linear theory.

[6] A generalisation to include surface currents can be made without much difficulty by applying the boundary conditions described by Friedberg [24], p 356–358.

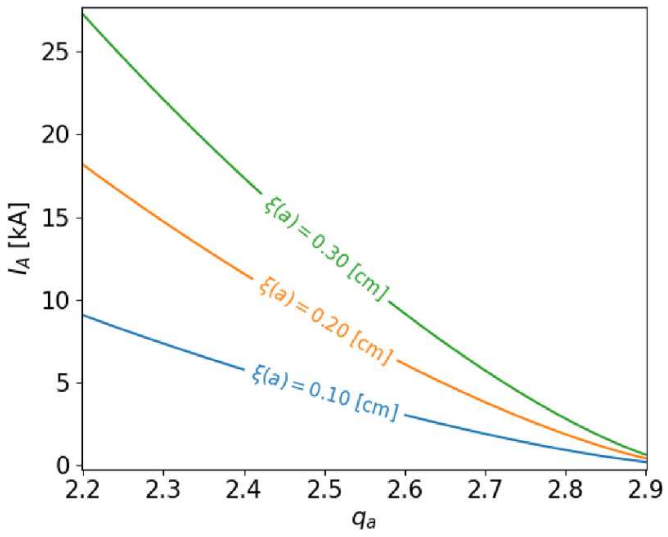

Figure 6. Necessary current in the antenna to obtain a saturated external kink mode of different amplitudes as a function of the edge safety factor q_a.

3.2. Comparison with 3D states calculated with the VMEC code

Now that we have calculated the saturated amplitude of external kinks in the presence of an antenna producing a single helicity MP, we proceed to verify numerically that the physics included in our linear estimation can describe some of the main features of the saturated external kink modes. This is done by calculating the equilibrium states using the VMEC code under the application of MPs.

The calculation of 3D saturated states in VMEC follows the procedure outlined in [14, 15]. In summary, a free boundary VMEC equilibrium is calculated in 3D geometry along with its neighbouring axisymmetric state, where the later is obtained by restricting $n = 0$ toroidal modes in the VMEC Fourier expansion. Then, the nonlinear normal saturated plasma displacement is calculated by subtracting the 3D surface from the 2D surface at each location in the normal direction of the 2D surface. It is pointed out that saturated external kink modes have already been successfully obtained using the VMEC code [14].

Following the analytical example outlined above, we use a Wesson-like current profile, with $q_0 = 1.2$ so that a cylindrical plasma would be external kink unstable in the interval $2.95 < q_a < 3$. The pressure profile is given by $P(s) = P_0(1 - s^2)$, where $P_0 = \beta_0 B_0^2/(2\mu_0)$ with $\beta_0 = 0.02$ and $B_0 = 2.7T$. Here, $s = \sqrt{\psi_t/\psi_{t_{\text{edge}}}}$. Both the safety factor and pressure profiles are plotted in figure 7. An almost circular cross section ($\kappa \sim 1.2$, $\delta \sim 0.125$, with κ, δ being elongation and triangularity respectively) is used to improve the comparison with the analytical results. Figure 7(b) shows the LCFS at different toroidal angles for the case of $q_a = 2.8$, where we note that there is a weak 3D perturbation.

The Fourier decomposition of the nonlinear saturated displacement (η_{mn}) is plotted in figure 8(a) for $q_a = 2.8$ without the application of MPs, showing that the 3D state does indeed correspond to a saturated external kink. Note in particular that the coupling between poloidal modes is very weak, as the main $(m = 3, n = 1)$ external kink strongly dominates the spectrum. This makes our comparison with the analytical model more viable. We clarify that the saturated states calculated without MPs adopt a completely axisymmetric vacuum magnetic field, but an initial perturbation on the magnetic axis guess is necessary to steer VMEC towards a converged 3D state [26, 27].

Figure 8(b) shows the saturated amplitude of the $(m = 3, n = 1)$ nonlinear displacement as a function of q_a. A small saturated displacement exists between $2.7 < q_a < 3.1$ in the absence of MPs. This corresponds to a somewhat broader region than the range over which the analytical cylindrical model is unstable. Therefore, a comparison with the analytical model should consider $q_a < 2.7$. It can be seen that the amplitude of the saturated plasma displacement increases with the current applied to the EFCCs, and moreover, the parameter space where such equilibrium modes can be obtained is also expanded with the application of the non-axisymmetric MPs, consistent with our linear equilibrium theory (figure 6).

To make a quantitative comparison between the analytical model and the 3D saturated states obtained in VMEC, we plot the amplitude of the saturated $(m = 3, n = 1)$ as a function of the vacuum radial perturbed magnetic field calculated through equation (8) for the linear analytical model, and through equation (7) for the full nonlinear VMEC equilibria. The amplitude of the linear equilibrium displacement (ξ) is plotted as dashed lines, while the amplitude of the nonlinear saturated state (η) is plotted as points for each of the different VMEC simulations. As shown in figure 9, good agreement between the two approaches is obtained for cases where the axisymmetric equilibrium is stable in the absence of MPs. Three important implications can be derived from this result. The first one is that non-resonant saturated external perturbations can be accurately modelled with linear theory in the frame of ideal MHD provided that the mode is stable or only weakly unstable in the absence of MPs. The second one is that MPs could be used to expand the parameter space for the saturation of external instabilities. The third one is that since good agreement is found between the full nonlinear solution and the simplified one in cylindrical geometry, poloidal coupling of the plasma response with different harmonics of the MPs does not seem to be important, at least when the effect of the MPs is dominant. Finally, we point out that agreement between the analytical model and VMEC for cases where the equilibrium is external kink-unstable in the absence of MPs was not obtained, which is in line with our previous prediction that the linear equilibrium model is inconsistent due to the absence of plasma inertia and the 3D nonlinear corrections associated with nonlinear saturation in the absence of the antenna. Instead, the MPs seem to enhance amplitude of the existent saturated external kink, as shown in figure 8(b).

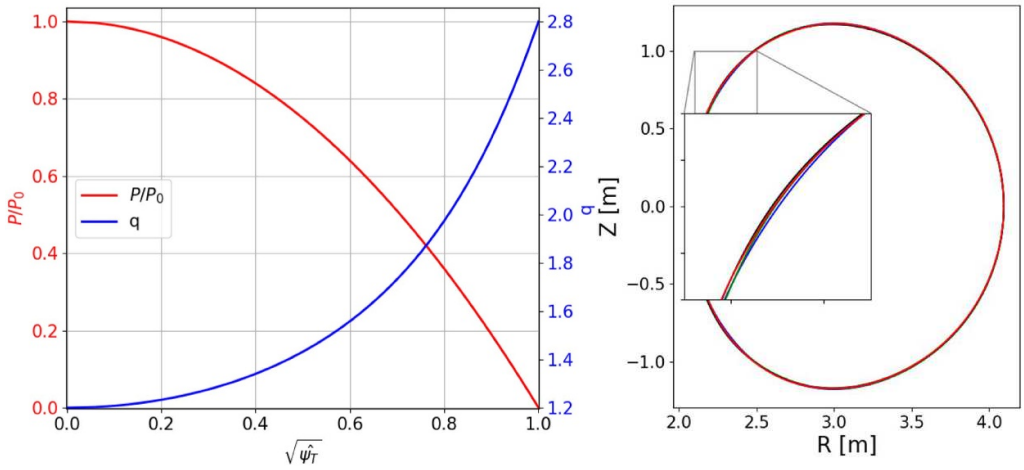

Figure 7. (a) Safety factor and pressure profiles of a `VMEC` equilibrium with a Wesson-like current density profile and (b) corresponding LCFS at different toroidal angles. Note that there is a weak 3D perturbation visible by the mismatched surfaces.

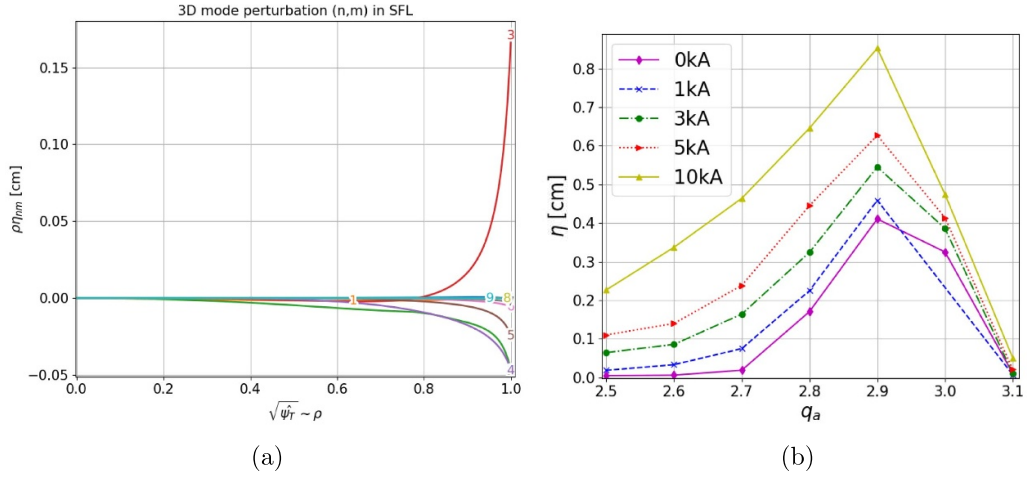

Figure 8. (a) Poloidal spectrum of the nonlinear saturated plasma displacement with $n = 1$ for a Wesson-like current density profile, with $q_0 = 1.2$ and $q_a = 2.8$.(b) $(m = 3, n = 1)$ Fourier component of the nonlinear saturated plasma displacement calculated in `VMEC` at different applied currents as a function of the value of the edge safety factor q_a.

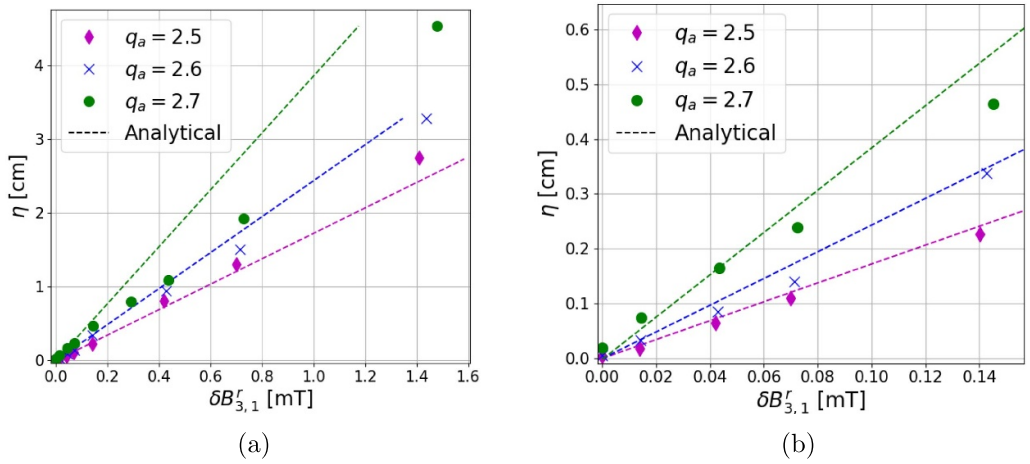

Figure 9. (a) Saturated amplitude of the external kink mode at the plasma edge as a function of the single helicity radial perturbed magnetic field. `VMEC` calculation (shown by the markers) is compared with the analytical estimation of our linear model (dashed lines) in equation (13). (b) Zoom over the region where the saturated amplitude is small, and thus where the analytical model is more valid.

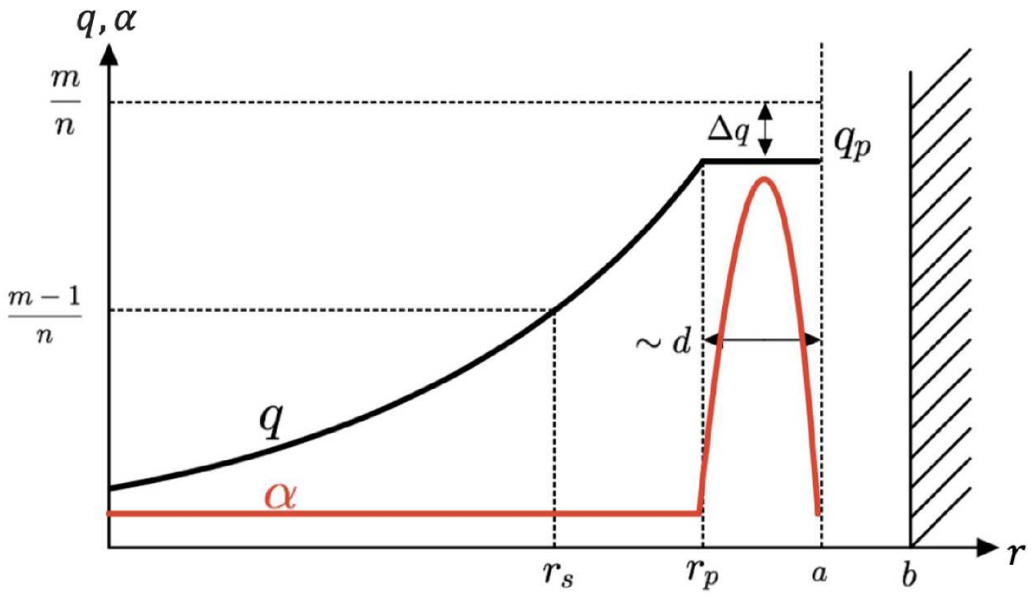

Figure 10. Cartoon of the profiles considered in the equilibrium model.

4. MP-induced saturated exfernal modes

Infernal modes are MHD instabilities that occur in plasmas where an extended region of low magnetic shear (with the safety factor close to a resonance, though the exact resonance is not required) coincides with a region with large pressure gradient. If such region of low magnetic shear is located near the edge, the upper sidebands of the main infernal mode can connect to the vacuum and trigger an external instability. Infernal external (*infernal*) modes result from the coupling of an infernal drive located in the pedestal region with its upper sideband external kink drive. The onset of exfernal modes has been linked to the saturated edge localised modes observed during QH-mode operation [28, 29]. As has been shown in the previous section, saturated external kink modes can be induced by the use of externally applied MPs, so it is expected that MPs have a similar effect on exfernal modes as well.

4.1. Linear equilibrium equation for exfernal modes with MP

The equilibrium under consideration models the key aspects observed during a QH-mode discharge, as seen in a simplified cartoon in figure 10. The pressure profile sits on a pedestal located near the plasma edge, creating a region of high pressure gradient ($\alpha = -\frac{2\mu_0 P' q^2}{B_0^2}$ is the ballooning α parameter). The safety factor monotonically increases in the region $r \in [0, r_{\rm p}]$, where $r_{\rm p}$ is the radius of the pedestal top. Then the safety factor is flat in the region $r \in [r_{\rm p}, a]$ as a consequence of the large edge bootstrap current generated in the low collisionality regime. The value of the safety factor plateau is located near a rational surface, i.e. $q = m/n + \Delta q$, where $|\Delta q| \ll 1$. It is pointed out that Δq can be positive or negative.

The antenna is again placed in the vacuum region, between the plasma boundary and the ideal wall. We separate the plasma into two regions, a high-shear and a low-shear region. The physics involving the exfernal drive is on the low-shear region, located at the plasma pedestal. The equation describing an exfernal time-invariant perturbation with mode number (m, n) is given by [30–32]

$$\frac{\mathrm{d}}{\mathrm{d}r}\left[r^3\left(\frac{1}{q}-\frac{1}{q_{\rm s}}\right)^2\frac{\mathrm{d}}{\mathrm{d}r}\xi_m\right] + \left[\left(1-m^2\right)\left(\frac{1}{q}-\frac{1}{q_{\rm s}}\right)^2 + \frac{\alpha}{q^2}\frac{r}{R_0}\left(\frac{1}{q^2}-1\right)\right] r\xi_m + \frac{\alpha}{2q^2}\left[\frac{r^{1+m}}{1+m}L_+ + \frac{r^{1-m}}{1-m}L_-\right] = 0, \tag{14}$$

where $q_{\rm s} = m/n$ and the constants $L_\pm$ appear after integration and substitution of the sideband equations

$$\left(r^{2\pm m}\xi_{m\pm1}\right)' = L_\pm r^{1\pm 2m} + \frac{1\pm m}{2} r^{1\pm m}\alpha\xi_m. \tag{15}$$

Note that the saturated amplitude of the main mode and of the sidebands is in force balance with the applied external MP. The solution to equation (14) gives the linear equilibrium amplitude of the main mode in terms of the applied current in the antenna, which is embedded in the constants $L_\pm = L_\pm(I_A)$. It is therefore necessary to calculate the constants $L_\pm$ in terms of the saturated amplitude of the main mode $\xi_m(r)$. Evaluation of equation (15) at $r = r_{\rm p}$ and $r = r_a$ gives

$$\xi_{m\pm1}(r_\mathrm{p}) = \frac{r_p^{\pm m} L_\pm}{2 \pm m + \mathcal{C}_\pm}$$
$$\xi_{m\pm1}(a) = \frac{a^{\pm m} L_\pm}{2 \pm m + \mathcal{B}_\pm}, \tag{16}$$

where $\mathcal{C}_\pm = r_\mathrm{p}\xi'_{m\pm1}(r_\mathrm{p})/\xi_{m\pm1}(r_\mathrm{p})$ is calculated from the cylindrical solution of the sideband equations in the low-shear region: $r \in [0, r_\mathrm{p}]$. Assuming Dirichlet boundary conditions for the main mode at $r = r_\mathrm{p}$ and $r = a$ [16, 32], the function $\mathcal{B}_\pm = a\xi'_{m\pm1}(a)/\xi_{m\pm1}(a)$ takes the same form as equation (12). Note that the vacuum MP is now assumed to be composed of two different harmonics corresponding to the upper and lower sideband helicities. The main harmonic is only affected by the MPs through coupling with the sidebands since the Dirichlet boundary condition at $r = a$ prohibits a direct effect from the vacuum perturbation. Integrating equation (15) in the interval $[r_\mathrm{p}, a]$ gives

$$r^{2\pm m}\xi_{m\pm1}\Big|_{r_\mathrm{p}}^{a} = \frac{r^{2(1\pm m)}L_\pm}{2(1\pm m)}\Big|_{r_\mathrm{p}}^{a} + \frac{1\pm m}{2}\int_{r_\mathrm{p}}^{a} \alpha r^{1\pm m}\xi_m \mathrm{d}r. \tag{17}$$

Finally, equations (12), (16) and (17) are solved for the constants $L_\pm$

$$L_\pm = \frac{a^{-2(1\pm m)}(1\pm m)^2(2\pm m+\mathcal{C}_\pm)\left[(2\pm m+\mathcal{B}_\pm)\epsilon\mathcal{D}_\pm \pm 2a^{2\pm m}H_\pm \frac{I_A\mu_0}{B_0}\right]}{\epsilon\left[(2\pm m+\mathcal{C}_\pm)(\pm m-\mathcal{B}_\pm) - (r_*/a)^{2(1\pm m)}(\pm m-\mathcal{C}_\pm)(2\pm m+\mathcal{B}_\pm)\right]}, \tag{18}$$

where $\mathcal{D}_\pm = \int_{r_\mathrm{p}}^{a} \alpha r^{1\pm m}\xi_m \mathrm{d}r$ and we have redefined

$$H_\pm = \frac{\left[1-(b/c)^{2(m\pm1)}\right](a/b)^{m\pm1}}{\left[(m\pm1)/q_\mathrm{a} - n\right]\left[1-(a/c)^{2(m\pm1)}\right]}$$
$$\mathcal{B}_\pm = \lim_{I_A\to0} a\frac{\xi'_{m\pm1}(a)}{\xi_{m\pm1}(a)}. \tag{19}$$

It is noted that in the limit of $I_A \to 0$, the definition of the constant $L_\pm$ from previous papers is recovered [30–32]. The amplitude of the antenna-driven, linearised equilibrium exfernal mode is obtained by the solution of equation (14), which is an integro-differential equation for $\xi_m(r)$ in the region $r \in [r_\mathrm{p}, a]$. Such an equation would typically be solved numerically. Nevertheless, a rough estimate of the linear equilibrium amplitude can be obtained by assuming a simplified pressure profile [32]: $\alpha \propto P' = -P_\mathrm{p}\delta(r - r_*)$ with $r_\mathrm{p} < r_* < a$. We then have $\mathcal{D}_\pm = \hat{\beta}_*\epsilon_*^{-1}r_*^{2\pm m}\xi_m(r_*)$, with $\hat{\beta}_* = 2P_*q^2/B_0^2$ and $\epsilon_* = r_*/R_0$. By writing the constants $L_\pm$ and I_ξ as

$$I_\xi = \frac{I_A\mu_0}{B_0\xi_m(r_*)}$$
$$L_\pm = (1\pm m)\, r_*^{\mp m}\epsilon_*^{-1}\xi_m(r_*)\left(\Lambda_\pm\hat{\beta}_* + G_\pm H_\pm I_\xi\right), \tag{20}$$

where the constants $\Lambda_\pm$ are defined in a similar way as in [18, 31, 32]:

$$\Lambda_\pm = \frac{(1\pm m)^2\left[2\pm m+\mathcal{B}_\pm(r_\mathrm{p})\right]\left[2\pm m+\mathcal{B}_\pm(r_x)\right]r_x^{-2(1\pm m)}}{(\pm m-\mathcal{B}_\pm(r_x))\left[2\pm m+\mathcal{B}_\pm(r_\mathrm{p})\right] - \left(\frac{r_\mathrm{p}}{r_x}\right)^{2(1\pm m)}(\pm m-\mathcal{B}_\pm(r_\mathrm{p}))(2\pm m\mathcal{B}_\pm(r_x))}. \tag{21}$$

equation (14) can be integrated across r_* to give

$$I_\xi = -\frac{2\epsilon_*^2}{(H_+G_+ + H_-G_-)\hat{\beta}_*}\left(\frac{1}{2\epsilon_*^2}\hat{\beta}_*^{\,2}(\Lambda_+ + \Lambda_-) + \left[\!\left[\frac{r\xi'_m}{\xi_m}\right]\!\right]_{r_*}\frac{\Delta q^2}{q_\mathrm{s}^2} + \left(\frac{1}{q^2}-1\right)\hat{\beta}_*\right). \tag{22}$$

It is pointed out that in the limit of $I_A \to 0$, equation (22) satisfies the marginal stability equation for exfernal modes [32]. In the open intervals $[r_\mathrm{p}, r_*)$ and $(r_*, a]$, the equation for ξ_m (14) reduces to Newcomb's equation (9) with $k_\parallel = constant$, and the solution takes a very simple form (equation (5.8) in [32]), leading to

$$\left[\!\left[\frac{r\xi'_m}{\xi_m}\right]\!\right]_{r_*} = \frac{2m\left[(r_*/r_\mathrm{p})^{2m} - (r_*/a)^{2m}\right]}{\left[(r_*/r_\mathrm{p})^{2m}-1\right]\left[(r_*/a)^{2m}-1\right]} \sim -\frac{2(a+r_\mathrm{p})}{a-r_\mathrm{p}}. \tag{23}$$

To evaluate equation (22) it is necessary to solve Newcomb's equation in the high-shear region to calculate the constants $\mathcal{C}_\pm$. For that purpose, the following shape of the safety factor profile is used

$$q(r) = \begin{cases} \frac{q_0(\kappa+n)}{\kappa[1-(r/r_-)^\mu]+n} & \text{if } r \in [0, r_\mathrm{p}] \\ q_\mathrm{p} & \text{if } r_\mathrm{p} \leqslant r \leqslant a, \end{cases} \tag{24}$$

where m, n are the poloidal and toroidal mode numbers of the main infernal mode, r_- roughly defines the radius of the lower sideband rational surface, q_0 is the safety factor at the magnetic axis, μ defines how peaked the profile is, and the constant κ guarantees the continuity of the profile at $r = r_\mathrm{p}$.

For the numerical calculation let us consider $a = 1.14$ m, $b = 2.40$ m, $c = \infty$, $\epsilon_* = 0.40$, $r_\mathrm{p}/a = 0.95$, $r_-/a = 0.85$, $B_0 = 2.5$ T, $\mu = 0.6$ and $q_0 = 1.2$, which roughly correspond to the JET-like QH-mode plasma calculated in the next section. Figure 11 shows the antenna current as a function of the value of Δq and $\hat{\beta}_*$, corresponding to the evaluation of equation (22) for different values of the linearised equilibrium amplitude. It is pointed out that all curves converge to zero at $\Delta q \sim -0.1$ in figure 11(a), and at $\hat{\beta}_* = 5.2\%$ in figure 11(b). These points in

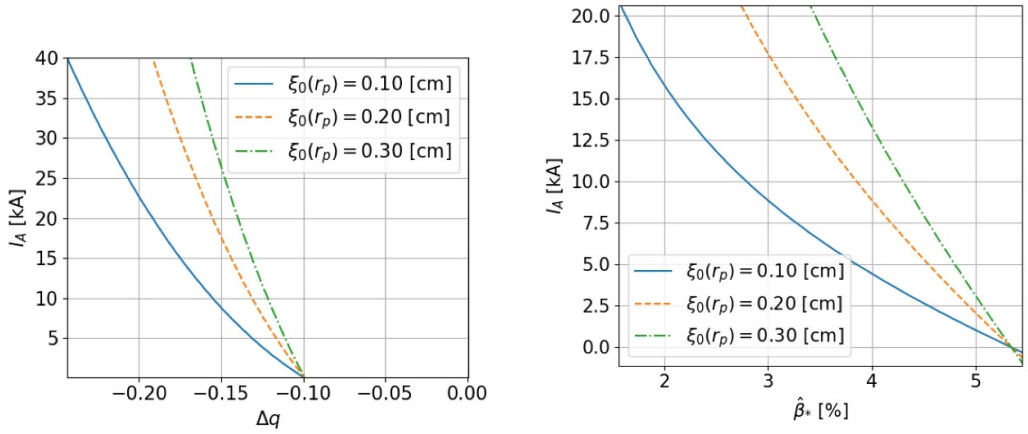

Figure 11. Necessary current in the antenna to obtain a saturated exfernal mode of different amplitudes as a function of (a) the distance to the rational surface in the pedestal (Δq) and (b) the value of $\hat{\beta}_*$. Figure (a) considers $\hat{\beta}_* = 0.045$, and figure (b) considers $\Delta q = -0.12$.

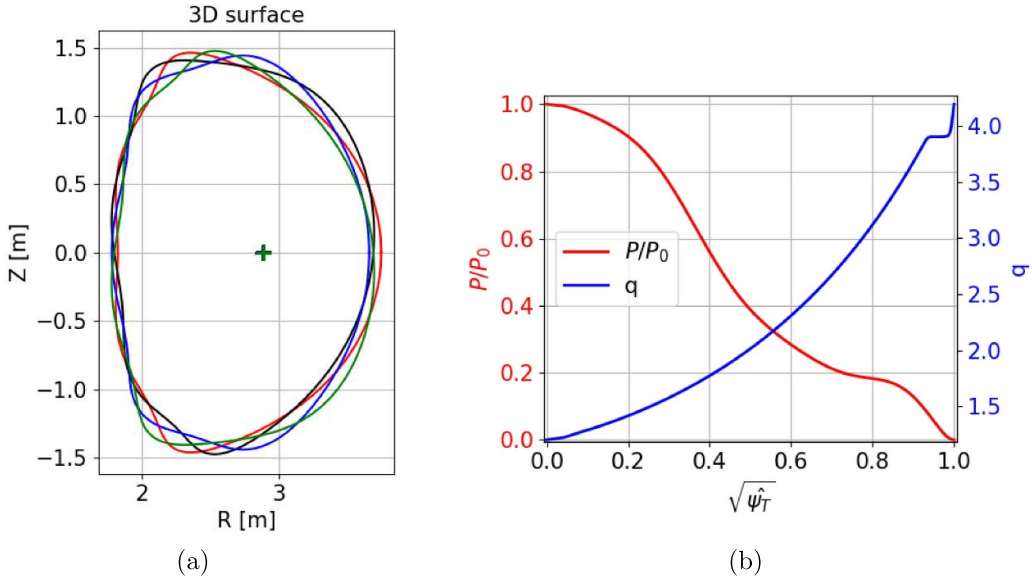

Figure 12. (a) LCFS at equally spaced ($\pi/2$). toroidal angles in QH-mode equilibrium with $q_{\rm p} = 3.98$ and without the application of MPs. (b) Pressure and safety factor profiles in `VMEC`.

the parameter space correspond to the marginally stable points in the absence of MPs.

4.2. Comparison with 3D states calculated with the `VMEC` code

For the comparison in this section, a more realistic QH-mode-like equilibrium is investigated, which is plotted in figure 12. Note that the safety factor is the same as in the analytical model given by equation (24), with the exception of the spike at the edge that takes the value of $q_{\rm a}$ above the $(m = 4, n = 1)$ rational surface. The effect of such a spike on the stability of the plasma does not significantly affect the saturated state of the exfernal mode [16], and the particular consequences of the spike on the interaction with external MPs will be discussed below. Figure 12(a) shows the LCFS of the 3D saturated equilibrium at different toroidal angles in the absence of MPs, revealing a strong 3D distortion of the plasma edge. Such 3D distortion corresponds to a saturated exfernal mode, which is speculated to be the EHOs observed during QH-mode operation. The large amplitude of the saturated mode found by `VMEC` is similar to what it was found in previous studies of QH-mode operation in JET-like plasmas [14, 16].

A quantitative comparison between the analytical equilibrium model and the `VMEC` results is more challenging for this more advanced case because of a number of reasons. Firstly, due to all the simplifications in the derivation of equation (22) (step-like pressure profile, flat safety factor, etc). Secondly, the vacuum perturbed magnetic field affecting each of the sideband harmonics scales differently in both approaches, i.e. $\frac{\delta B^r_{\rm EFCC}(m-1,n)}{\delta B^r_{\rm EFCC}(m+1,n)} \neq \frac{\delta B^r_{\rm antenna}(m-1,n)}{\delta B^r_{\rm antenna}(m+1,n)}$. This is because in the analytical model the vacuum perturbed magnetic field scales with the

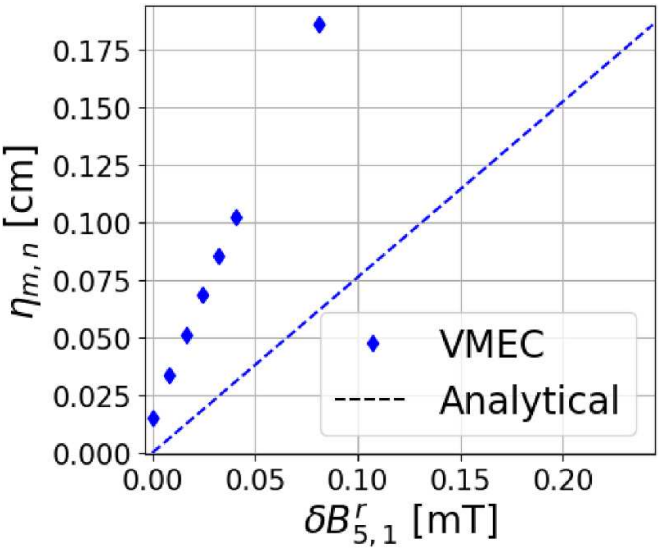

Figure 13. Saturated amplitude of the main infernal mode $(m = 4, n = 1)$ at the pedestal calculated in VMEC and in the analytical model as a function of the $(m = 5, n = 1)$ Fourier component of the vacuum radial perturbed magnetic field. The value of the safety factor plateau is $q_{\rm p} = 3.88$, where the mode is stable and very close to marginal stability in the absence of MPs.

poloidal mode number m as given by equation (8), while in VMEC it follows the EFCC poloidal geometry (figure 5). Nevertheless, examination of the linear eigenfunctions of marginal cases without the application of MPs show that the lower sideband vacuum connection is also weak. Therefore, we can neglect the effect of MPs on the lower sideband and only consider the $(m+1, n)$ Fourier component of the vacuum radial perturbed field in both approaches. Thirdly, the value of the safety factor at the boundary is different in both approaches since the analytical model does not require a spike at the plasma edge. Note that the coupling between the upper sideband external kink drive with the MPs is highly sensitive to the value of $q_{\rm a}$. Finally, in the analytical model the main (m, n) mode in the pedestal is not *directly* affected by the MP due to the imposed boundary condition at the plasma-vacuum interphase (note that *indirect* coupling of the main mode with the MPs is still present through interaction with the sidebands), while in VMEC the edge plasma surface is free to move and the equilibrium solution is self-consistent with the applied MPs for all the modes. While some of these difficulties could be avoided by numerically solving the integro-differential equation (14), a direct evaluation of our analytical estimation (22) gives a rough approximation of the saturated amplitude.

In order to compare the two approaches we need to analyse an equilibrium that is linearly stable in the absence of MPs. We choose $q_{\rm p} = 3.88$, which corresponds to a point with vanishing nonlinear amplitude of the plasma displacement in the absence of MPs (see figure 14(a)). The comparison is shown in figure 13. We point out that the vacuum radial perturbed field in the nonlinear numerical approach is only the one corresponding to the upper sideband helicity $(m = 5, n = 1)$. In the linear analytical approach, the current I_A in equation (22) is substituted by δB^r_{m+1} using equation (8). Then it is assumed that $G_+/G_- \ll 1$ (which for our case is $\sim 10^{-2}$) to isolate δB^r_{m+1} from the amplitude of the mode $\xi_m(r_*)$. The saturated amplitude in VMEC has a linear dependency on the $(m = 5, n = 1)$ component of the vacuum radial perturbed field, similar to the analytical model. Moreover, the calculated saturated amplitude of the plasma displacement in both approaches is of the same order of magnitude. We attribute the difference in slope primarily to the approximations outlined above, though some assumptions may have a stronger impact than others. As shown in [15] (figure 15), analytical growth rates for external modes calculated using similar profile assumptions are comparable to those obtained from realistic equilibria with the KINX code [33] in the absence of MPs, which suggests that the simplifications in the plasma profiles are expected to have a limited effect. Therefore, the dominant contribution likely comes from the different physics included on the MP modelling between the two approaches. In particular, the absence of direct coupling between the main (m, n) mode and the perturbed vacuum field is expected to have the strongest influence since the perturbation amplitude scales with MP coupling strength.

4.3. Beyond linear modelling: The extended parameter space of saturated exfernal modes

One of the main goals of this work is to verify that EHOs (or saturated exfernal modes) can be induced over a wider parameter space with the assistance of externally applied MPs. In the previous section it was shown using analytical and numerical approaches that MPs can indeed be used for such purposes. Now we go beyond the validity of the linear model and analyse the effect of MPs also in cases where the plasma is exfernal-unstable in the absence of MPs. Figure 14(a) shows the saturated amplitude of the main infernal $(m = 4, n = 1)$ mode at the pedestal as a function of the value of the safety factor plateau $q_{\rm p}$ and magnetic shear s over the pedestal region. A significant expansion of the parameter space is observed for both

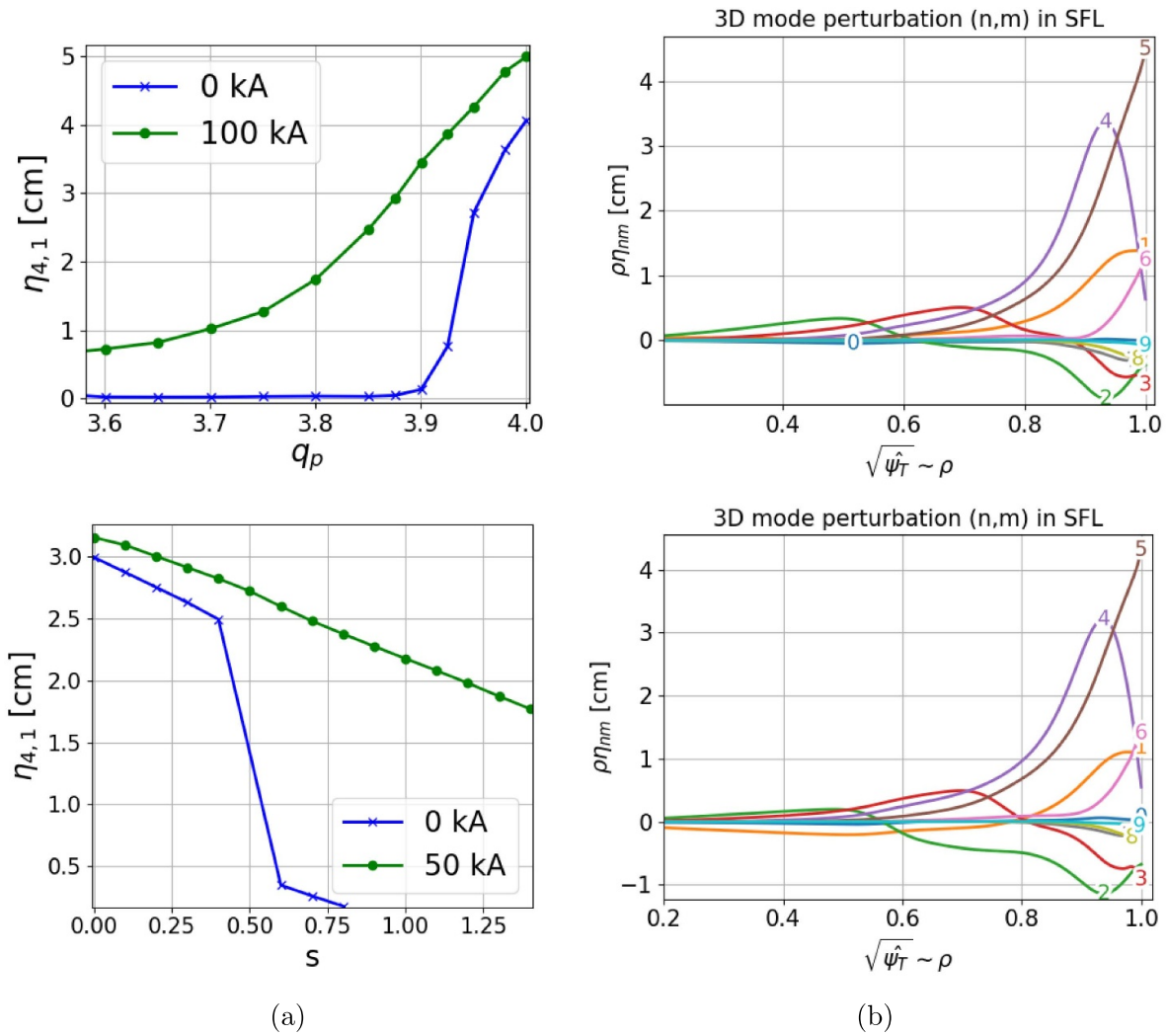

Figure 14. (a) Peak of the $(m = 4, n = 1)$ Fourier component of the nonlinear plasma displacement evaluated at the pedestal as a function of the value of the safety factor plateau (up) and (b) of the magnetic shear (bottom). (b) Poloidal Fourier spectrum (with $n = 1$) of the nonlinear plasma displacement with flat safety factor and $q_{\rm p} = 3.98$ and 0 kA (up), and with $q_{\rm p} = 3.90$ and 100 kA (bottom).

parameter scans. Since the amplitude of the saturated modes is not small anymore, the validity of the linear model is limited even for the cases where the exfernal modes were induced only by the MPs (i.e. cases that are exfernal-stable in the absence of MPs). Still, it is possible to check that the same exfernal mode is excited with and without MPs at different regions of the parameter space by analysing two equilibria with similar amplitude with and without MPs. Figure 14(b) shows the poloidal Fourier spectrum of the nonlinear saturated plasma displacement for $q_{\rm p} = 3.98$ at 0 kA, and for 3.90 at 100 kA. As can be seen, the exact same mode is observed, confirming that the parameter space of static exfernal modes is expanded by the application of MPs.

5. Summary and conclusions

Two approaches to model non-axisymmetric MPs in tokamak plasmas have been presented. The first one invokes the analytical model developed in [4], which corresponds to an antenna located in the vacuum region in between the plasma surface and an ideal wall. The current in the antenna produces a perturbed helical magnetic field, which modifies the boundary conditions of the linearised ideal MHD equilibrium equations. The second method uses a set of non-axisymmetric coils, where the vacuum magnetic field is evaluated numerically through Biot–Savart law. The vacuum field is then used to calculate a nonlinear equilibrium state in the `VMEC` free boundary code. We point out that in both approaches the obtained plasma displacement is in force balance with the applied MPs, so the plasma response is automatically included in the solution. To make a quantitative comparison of the applied MP, in the nonlinear `VMEC` approach the radial perturbed vacuum field is Fourier decomposed in SFL coordinates using the geometry of the axisymmetric equilibrium. Then, the amplitude of the helical component of interest is compared with the radial vacuum field of the antenna calculated in the absence of a plasma.

On a first instance, both approaches to model the MPs were applied to the case of a saturated external kink. It was found

that such saturated modes can be induced by the application of MPs, and the saturated amplitude of the plasma displacement is in quantitative agreement in both approaches for parameters for which the plasma is linearly stable in the absence of MPs. This means that, within the approximations of the ideal MHD model, there is a good understanding of the mechanism that describes the effect of the applied perturbed field on non-resonant external modes. On a second instance we also model equilibrium states with MPs for the case of saturated exfernal modes, assumed here to be the EHOs observed during QH-mode operation. For this more complex case quantitative agreement was limited, with both approaches giving the same order of magnitude of the saturated plasma displacement as well as a similar linear dependency of the amplitude on the applied MP.

Finally, the VMEC code was used to estimate the increase of the parameter space of saturated EHOs with the application of MPs. An extensive parameter scan was performed with respect to the value of the safety factor at the plateau and the magnetic shear in the pedestal. In both cases it was found that a significant increase in the parameter space can be achieved by the application of MPs. By analysing the Fourier spectrum of the saturated amplitude in equilibria with and without the application of MPs at different locations of the parameter space, it was concluded that the same mode can be excited with the help of MPs. This important results points to the possibility of using external non-axisymmetric coils as an actuator to access weakly 3D plasma states in advanced operational regimes such as QH-mode operation.

Data availability statement

All data that support the findings of this study are included within the article (and any supplementary files).

ORCID iDs

G Bustos-Ramirez 0009-0000-0509-0904
J P Graves 0000-0002-7959-7959
D Brunetti 0000-0001-8650-3271

References

[1] Burrell K H *et al* 2004 Edge radial electric field structure in quiescent H-mode plasmas in the DIII-D tokamak *Plasma Phys. Control. Fusion* **46** A165–78
[2] Evans T E *et al* 2004 Suppression of large edge-localized modes in high-confinement DIII-D plasmas with a stochastic magnetic boundary *Phys. Rev. Lett.* **92** 235003
[3] Okabayashi M *et al* 2005 Control of the resistive wall mode with internal coils in the DIII–D tokamak *Nucl. Fusion* **45** 1715
[4] Lazzaro E and Nave M F F 1988 Feedback control of rotating resistive modes *Phys. Fluids* **31** 1623
[5] Liu Y, Kirk A and Nardon E 2010 Full toroidal plasma response to externally applied nonaxisymmetric magnetic fields *Phys. Plasmas* **17** 122502
[6] Yadykin D, Gryaznevich M, Frasinetti L and Gerasimov S 2014 Effect of the external helical fields on the plasma boundary shape in JET *Nucl. Fusion* **54** 013016
[7] Cooper W A *et al* 2015 Free boundary equilibrium in 3D tokamaks with toroidal rotation *Nucl. Fusion* **55** 063032
[8] King J D *et al* 2015 Experimental tests of linear and nonlinear three-dimensional equilibrium models in DIII-D *Phys. Plasmas* **22** 072501
[9] Orain F *et al* (the ASDEX Upgrade Team and the EUROfusion MST1 Team) 2017 Non-linear modeling of the plasma response to RMPs in ASDEX Upgrade *Nucl. Fusion* **57** 022013
[10] Fitzpatrick R 2018 Two-fluid nonlinear theory of response of tokamak plasma to resonant magnetic perturbation *Phys. Plasmas* **25** 112505
[11] Turnbull A D 2012 Plasma response models for non-axisymmetric perturbations *Nucl. Fusion* **52** 054016
[12] Turnbull A D *et al* 2013 Comparisons of linear and nonlinear plasma response models for non-axisymmetric perturbations *Phys. Plasmas* **20** 056114
[13] Hirshman S P and Whitson J C 1983 Steepest-descent moment method for three-dimensional magnetohydrodynamic equilibria *Phys. Fluids* **26** 3553–68
[14] Kleiner A, Graves J P, Cooper W A, Nicolas T and Wahlberg C 2018 Free boundary 3D ideal MHD equilibrium calculations for non-linearly saturated current driven external kink modes in tokamaks *Nucl. Fusion* **58** 074001
[15] Kleiner A, Graves J P, Brunetti D, Cooper W A, Medvedev S, Merle A and Wahlberg C 2019 Current and pressure gradient triggering and nonlinear saturation of low- n edge harmonic oscillations in tokamaks *Plasma Phys. Control. Fusion* **61** 084005
[16] Bustos-Ramirez G, Graves J P and Brunetti D 2021 Edge Harmonic Oscillations in plasmas with a separatrix and the effect of edge magnetic shear *Plasma Phys. Control. Fusion* **63** 124004
[17] Lazerson S A, Loizu J, Hirshman S and Hudson S R 2016 Verification of the ideal magnetohydrodynamic response at rational surfaces in the VMEC code *Phys. Plasmas* **23** 012507
[18] Brunetti D, Graves J P, Lazzaro E, Mariani A, Nowak S, Cooper W A and Wahlberg C 2018 Analytic stability criteria for edge MHD oscillations in high performance ELM free tokamak regimes *Nucl. Fusion* **58** 014002
[19] Lazerson S, Schmitt J, Zhu C, Breslau J and Developers A S 2020 Stellopt *Computer software* https://doi.org/10.11578/dc.20180627.6
[20] Barlow I, Bigi M, Bird J, Bonizzoni G, and Buttery R The error field correction coils on the JET machine EURATOM/UKAEA *Technical Report*
[21] Boozer A H 2001 Error field amplification and rotation damping in tokamak plasmas
[22] Newcomb W A 1960 Hydromagnetic stability of a diffuse linear pinch *Ann. Phys., NY* **10** 232–67
[23] Reiman A *et al* 2015 Tokamak plasma high field side response to an N = 3 magnetic perturbation: a comparison of 3D equilibrium solutions from seven different codes *Nucl. Fusion* **55** 063026
[24] Freidberg J P 2014 *Ideal MHD* (Cambridge University Press) p 1
[25] Wesson J A 1978 Hydromagnetic stability of tokamaks *Nucl. Fusion* **18** 87–132
[26] Cooper W A, Graves J P, Pochelon A, Sauter O and Villard L 2010 Tokamak magnetohydrodynamic equilibrium states with axisymmetric boundary and a 3D helical core *Phys. Rev. Lett.* **105** 035003
[27] Cooper W A, Graves J P, Sauter O, Rossel J, Albergante M, Coda S, Duval B P, Labit B, Pochelon A and Reimerdes H 2011 Helical core tokamak MHD equilibrium states *Plasma Phys. Control. Fusion* **53** 124005

[28] Brunetti D, Graves J P, Lazzaro E, Mariani A, Nowak S, Cooper W A and Wahlberg C 2019 Excitation mechanism of low- n edge harmonic oscillations in edge localized mode-free, high performance, tokamak plasmas *Phys. Rev. Lett.* **122** 155003

[29] Zheng L J, Kotschenreuther M T and Valanju P 2013 Low-n magnetohydrodynamic edge instabilities in quiescent H-mode plasmas with a safety-factor plateau *Nucl. Fusion* **53** 063009

[30] Hastie R J and Hender T C 1988 Toroidal internal kink stability in tokamaks with ultra flat q profiles *Nucl. Fusion* **28** 585

[31] Gimblett C G, Hastie R J and Hender T C 1996 An analytic study of the magnetohydrodynamic stability of inverse shear profiles *Phys. Plasmas* **3** 3369–74

[32] Brunetti D, Graves J P, Lazzaro E, Mariani A, Nowak S, Cooper W A and Wahlberg C 2018 Analytic study on low-n external ideal infernal modes in tokamaks with large edge pressure gradients *J. Plasma Phys.* **84** 1–22

[33] Degtyarev L, Martynov A, Medvedev S, Troyon F, Villard L and Gruber R 1997 The KINX ideal MHD stability code for axisymmetric plasmas with separatrix *Comput. Phys. Commun.* **103** 10–27